ACS APPLIED MATERIALS & INTERFACES

Research Article

www.acsami.org

Enhanced Carrier Collection from CdS Passivated Grains in Solution-Processed $Cu_2ZnSn(S,Se)_4$ Solar Cells

Melanie Werner,*[,†,#] Debora Keller,[†,§,#] Stefan G. Haass,[†] Christina Gretener,[†] Benjamin Bissig,[†] Peter Fuchs,[†] Fabio La Mattina,[‡] Rolf Erni,[§] Yaroslav E. Romanyuk,[†] and Ayodhya N. Tiwari[†]

[†]Laboratory for Thin Films and Photovoltaics, [§]Electronics/Metrology/Reliability, and [‡]Electron Microscopy Center, EMPA—Swiss Federal Laboratories for Materials Science and Technology, Ueberlandstrasse 129, 8600 Duebendorf, Switzerland

Supporting Information

ABSTRACT: Solution processing of $Cu_2ZnSn(S,Se)_4$ (CZTSSe)—kesterite solar cells is attractive because of easy manufacturing using readily available metal salts. The solution-processed CZTSSe absorbers, however, often suffer from poor morphology with a bilayer structure, exhibiting a dense top crust and a porous bottom layer, albeit yielding efficiencies of over 10%. To understand whether the cell performance is limited by this porous layer, a systematic compositional study using (scanning) transmission electron microscopy ((S)TEM) and energy-dispersive X-ray spectroscopy of the dimethyl sulfoxide processed CZTSSe absorbers is presented. TEM investigation revealed a thin layer of CdS that is formed around the small CZTSSe grains in the porous bottom layer during the chemical bath deposition step. This CdS passivation is found to be beneficial for the cell performance as it increases the carrier collection and facilitates the electron transport. Electron-beam-induced current measurements reveal an enhanced carrier collection for this buried region as compared to reference cells with evaporated CdS.

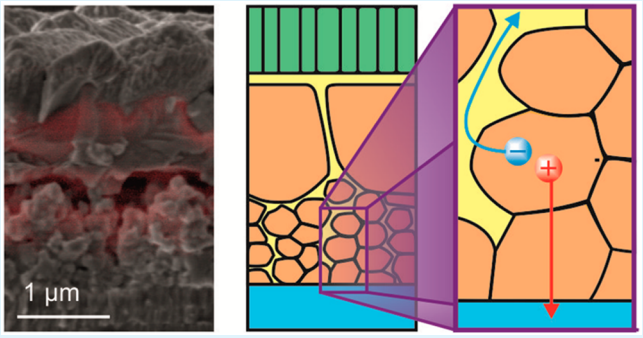

KEYWORDS: *thin film solar cells, kesterites, CdS, transmission electron microscopy, electron-beam-induced current*

INTRODUCTION

Nonvacuum processing remains very attractive for fabricating kesterite—$Cu_2ZnSn(S,Se)_4$ (CZTSSe) solar cells, taking into account that the currently highest efficiency of 12.7% has been achieved with a solution process using hydrazine as a solvent.[1] Alternative solvents, such as dimethyl sulfoxide (DMSO), can also be used as a safer alternative,[2] but such absorbers suffer often from a high porosity and a high surface roughness. After annealing the CZTS precursor under reactive selenium/sulfur, a bilayer structure with a dense top crust and a porous bottom layer is commonly observed.[3−6] It was suggested that the formation of the large top grains is due to the combination of the solid-state diffusion of Cu and Zn species and the vapor-phase supply of SnSe and Se.[6] Once a dense top crust is formed, it hinders further diffusion of the elements, and smaller grains remain at the bottom. Efficiencies of over 10% for such device structures were reported[7,8] and it was claimed that the porous bottom layer has no effect on the device performance.[9,10]

Here, we demonstrate that the porous bottom layer can contribute to the charge carrier collection and enhanced device efficiency. By (scanning) transmission electron microscopy ((S)TEM) analysis combined with energy-dispersive X-ray spectroscopy (EDX), we identify a CdS layer around the small grains in the porous bottom part and suggest that its formation is possible because of the penetration of solution, containing Cd^{2+} ions and thiourea, into the absorber during the chemical bath deposition (CBD). By optimization of the annealing conditions, an efficiency of over 10% was achieved.

EXPERIMENTAL SECTION

For CZTSSe absorber film preparation, thiourea (99%+ from Sigma-Aldrich), $SnCl_2$ (98% from Sigma-Aldrich), $ZnCl_2$ (99.99% from Alfa Aesar), $CuCl_2$ (98%+ from Alfa Aesar), and 0.1 M NaCl were dissolved in DMSO (99.9% from Alfa Aesar) not exceeding 3.5 M of total salt concentration, to target the metal ratios of Cu/(Sn + Zn) = 1.2 and Zn/Sn = 0.8. The precursor solution was spin-coated on Mo-coated soda lime glass substrate following a drying step at 320 °C on a hot plate for 1 min under atmospheric conditions. This step was repeated several times to build up the desired film thickness of the precursor. The precursor film was transferred to a rapid thermal process reactor (ANNEALSYS AS-One). The annealing of the precursor took place in a closed graphite crucible with 0.7 g of Se pellets placed around the sample. All samples were selenized under a nitrogen base pressure of 850 mbar for 15 min at 500 °C. ICP-MS gave a S/(S + Se) ∼ 0.15 for the CZTSSe absorbers. The CZTSSe absorbers were KCN-etched to remove possible binary phases. For solar cell fabrication, CdS was deposited either by CBD or by CdS evaporation. CdS-CBD was done by immersing the CZTSSe absorber

Received: March 19, 2015
Accepted: May 18, 2015
Published: May 18, 2015

DOI: 10.1021/acsami.5b02435
ACS Appl. Mater. Interfaces 2015, 7, 12141−12146

in an aqueous bath containing cadmium acetate, thiourea, and ammonia for 22 min at a temperature of 70 °C. Performed under similar conditions, by simply omitting the sulfur source thiourea, the so-called Cd-partial electrolyte (PE) treatment was done. The deposition of the CdS-PVD buffer took place in a high-vacuum system at 10^{-6} mbar by thermal-evaporating CdS pellets (Umicore, 5N). After the deposition of CdS, the samples were annealed for 2 min at 180 °C. Subsequently, an i-ZnO/ZnO:Al window bilayer was magnetron-sputtered, followed by mechanical scribing of individual cells of 0.09 and 0.3 cm^2. For the best cell a Ni–Al grid was deposited by electron-beam evaporation and a 105-nm-thick MgF_2 antireflection coating. Table 1 gives an overview of all samples and its buffer layer deposition method. The non-vacuum-processed CIS solar cell was fabricated from nanoparticle dispersion and is described elsewhere.[11]

Table 1. Overview of Absorber Material and Buffer Layer Deposition Method

sample	absorber	buffer layer deposition
A	CZTSSe	CdS-CBD
B	CZTSSe	CdS-PVD
C	CZTSSe	Cd PE
D	CIGS	CdS-CBD

The composition of CZTSSe layers was measured by X-ray fluorescence and EDX. The morphology was studied by SEM (FEI Nova NanoSEM230) and (S)TEM and EDX analysis was performed on a JEOL 2200FS TEM/(S)TEM operated at 200 kV. TEM specimens were prepared by in situ lamella lift-out on a FEI Helios NanoLab 600i DualBeam. A Pt/C layer was deposited as a protection coating. In the first milling stage, 30 kV Ga milling was applied, and then the voltage was reduced to 8, 5, 2, and 1 kV for the final milling. Electron beam induced current (EBIC) measurements on solar cells were performed in a FEI Strata 235 Dual Beam focused ion beam and secondary electron microscope at an acceleration voltage of 3 kV without applied bias. The current was measured with a SR570 Preamplifier from SRS at a gain of 10^7 A. An injection current of 36 pA was used. Injection level and energy were kept low to minimize possible artifacts related to the injection current.[12] Samples were prepared by mechanical cleaving and electrically contacting the front and back with silver paste and indium wires. The CZTSSe solar cell devices were characterized by J–V and external quantum efficiency measurements under standard test conditions (AM 1.5G spectrum, 25 °C, 1000 W/m^2).

RESULTS AND DISCUSSION

An overview of the samples described below is given in Table 1. A representative CZTSSe absorber morphology is shown in the scanning electron microscopy (SEM) image in Figure 1a,b. A bilayer structure with large grains on the top and smaller grains at the bottom is observed (Figure 1a). From the SEM top view image one can see that the top layer is not dense and some pinholes are visible. This device structure is typical for solution and nanoparticle processed CZTSSe absorbers and was described many times elsewhere.[5,9,10] The highest solar cell efficiency obtained for our absorber is 10.5% (with antireflective coating, 0.3 cm^2 cell area). The corresponding current–voltage (J–V) curve of the best performing cell is presented in Figure 1c.

(S)TEM/EDX studies on the CZTSSe solar cells were done, inter alia, to analyze the elemental distribution of the bilayer device structure. Figure 2a–c shows an SEM image (a) of the TEM lamella of such a CZTSSe solar cell device (sample A). The two layers (large grain at the top and smaller at the bottom) of the CZTSSe absorber can be clearly identified and the large grains do not extend into the porous layer. Many holes within the CZTSSe bottom layer are visible. The CZTSSe lamella was further thinned as shown in the overview bright-field (BF)-(S)TEM image (Figure 2b). To gain insights into the composition of the CZTSSe films, (S)TEM/EDX maps were collected of the sample area shown in Figure 2c. Figure 2d shows the corresponding Cu, Zn, Sn, S, Se, and Cd maps measured on the CZTSSe solar cell. The Sn L-lines and Cd L-lines overlap partially. Therefore, reference EDX spectra of Sn and Cd were used to separate the intensities of their signals by multiple linear least-squares fitting. The elemental distributions of Cu, Zn, Sn, and Se coincide, corresponding to the CZTSSe phase. Nevertheless, the presence of secondary phases cannot be excluded from these mappings. Importantly, an enrichment of S and CdS is found around the small grains. For a better visualization, the signals of all CZTSSe elements (blue) were compared with the signals of all CdS elements (red) in one map (Figure 2d), whereas the CZTSSe signal was approximated by the intensities (I), I(Cu)*I(Zn)*I(Sn)*I(S)*I(Se), and the signal of the CdS elements by I(Cd)*I(S). The CdS enrichment was confirmed by (S)TEM for different batches of CZTSSe solar cells with CBD-CdS buffer layers. We assume that the aqueous solution containing Cd^{2+} and thiourea is absorbed by the porous layer of the CZTSSe absorber and the penetration is accelerated due to capillary action. The formation of the solid CdS can take place even within the bottom layer of the absorber. After the buffer layer deposition an annealing step was done to evaporate all the remaining solution.

To verify the hypothesis that CdS is formed in the porous part from the liquid phase during CBD and not by solid-state

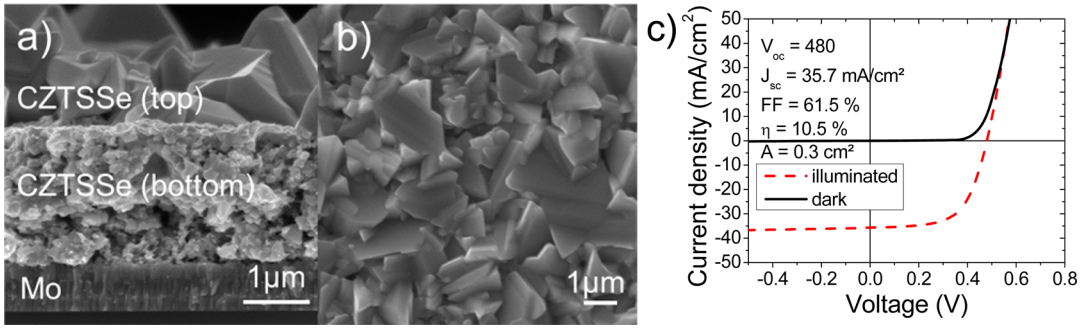

Figure 1. Typical SEM cross-section image (a) of a bilayer CZTSSe absorber and (b) top view. The segregation of the large crystals of the top layer and the porous bottom layer are clearly visible. (c) J–V characteristics of the best performing solar cell with a total area of 0.3 cm^2 under dark and illuminated conditions.

DOI: 10.1021/acsami.5b02435
ACS Appl. Mater. Interfaces 2015, 7, 12141–12146

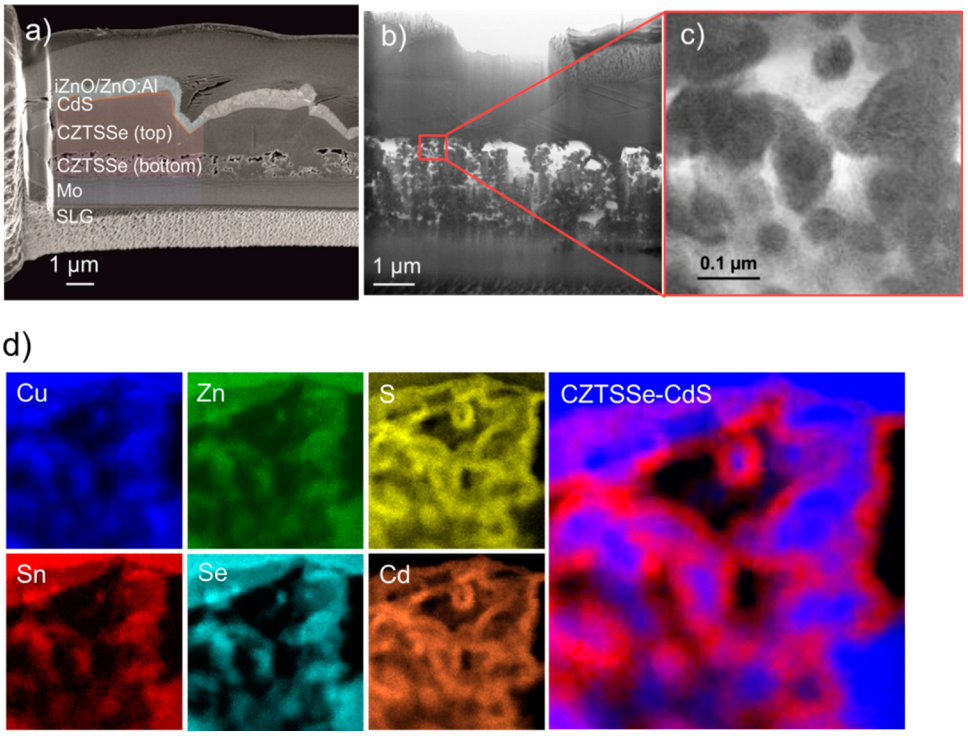

Figure 2. (a–c) SEM image in (a) of the TEM lamella of finished CZTSSe solar with CdS-CBD (sample A). Bright field-(S)TEM images of the analyzed region are shown in (b) and (c). The CZTSSe bottom layer is not dense and holes are visible within the layer. EDX maps of the elements Cu, Zn, S, Sn, Se, and CdS is shown in (d). An overlay of all acquired maps indicates the formation of CdS layer around the small grains in the bottom (CZTSSe-CdS).

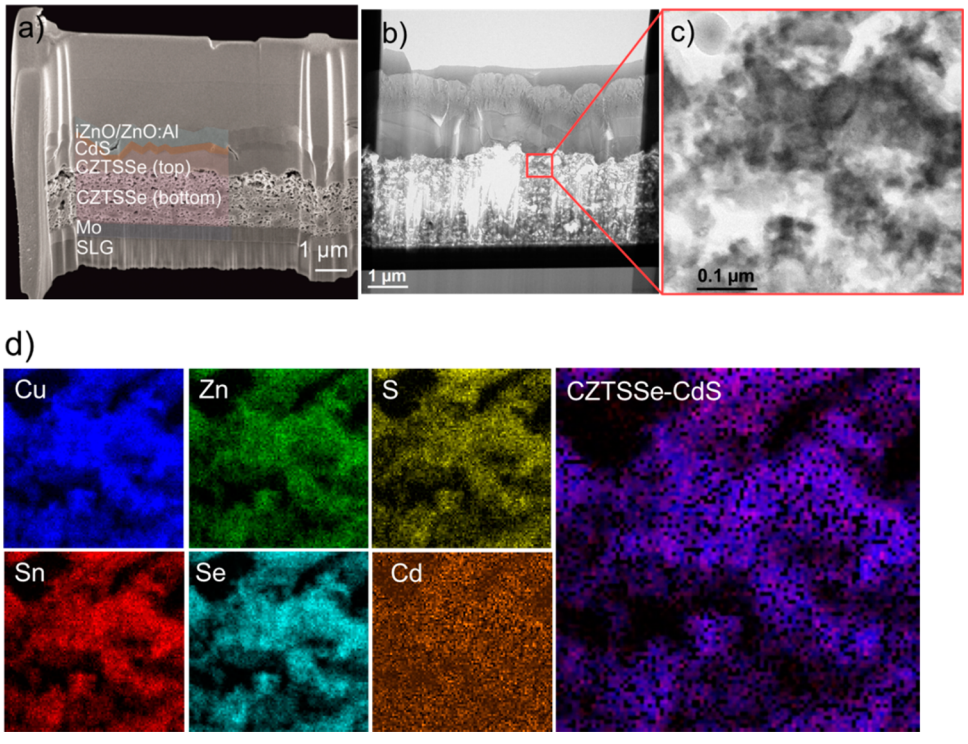

Figure 3. SEM image of finished solar cell lamella (sample B). CdS was deposited by PVD with a thickness of about 200 nm as indicated in (a). The TEM (bright field) images of the thinned out lamella and the enlarged area are presented in (b) and (c). The EDX maps (d) show a homogeneous distribution of Cu, Zn, Sn, S, and Se within the small grains of the CZTSSe bottom layer. No CdS was detected around the grains when CdS was deposited by PVD. The overlay of the maps (CZTSSe-CdS) gives no indication of the CdS formation.

diffusion, CdS was deposited by thermal evaporation (sample B) on a reference cell. Since the surface of the CZTSSe absorber is relatively rough, ~200 nm of CdS was deposited to ensure its complete coverage, yielding the highest device

DOI: 10.1021/acsami.5b02435
ACS Appl. Mater. Interfaces 2015, 7, 12141–12146

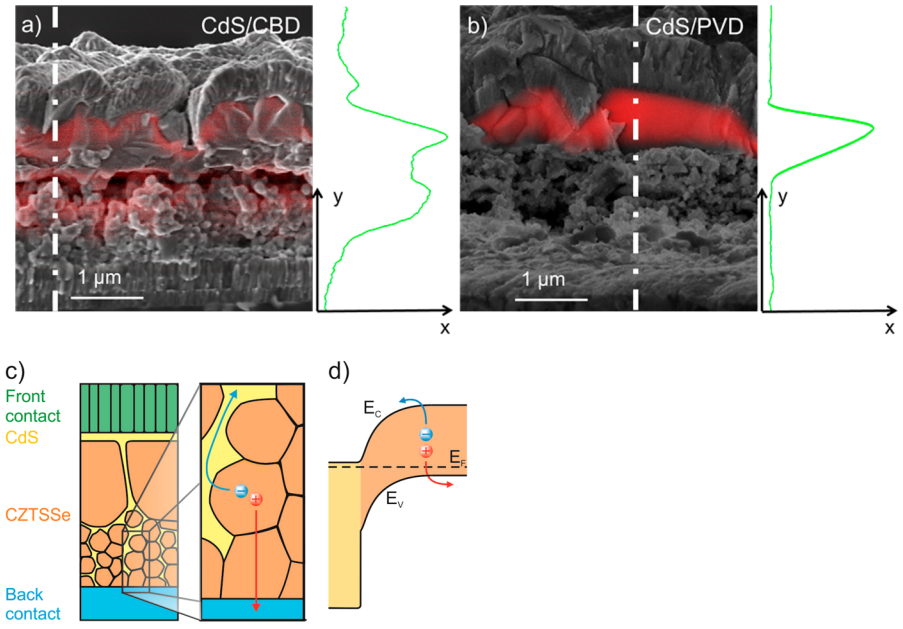

Figure 4. (a, b) EBIC signals (red area) overlaid with the SEM cross-sectional images of finished CZTSSe solar cell device. The integrated EBIC signal (green graphs) in *x*-direction taken along the dashed white lines. (a) Cleaved CZTSSe solar cell where CdS was deposited using CBD, the charge carrier collection expands from the large grains (top) to the small grains of the bottom layer. When CdS deposited by PVD, (b) the EBIC signal is narrower when compared with (a). Schematic of the bilayer CZTSSe absorber solar cell visualizes the CdS passivation of the grains in the bottom layer (c) and shows a possible band alignment of the local p−n junction at the small CZTSSe grain/CdS interface (d).

performance within an investigated range of CdS thickness between 100 and 400 nm. Again, a lamella of a sample with PVD-CdS was prepared for TEM analysis (Figure 3a−c). The elemental (Cu, Sn, Zn, S, Sn) distribution in sample B is homogeneous and equivalent to the previous sample (Figure 3d). This is expected since the CZTSSe absorber fabrication remains the same. One can immediately identify the difference in the EDX Cd maps. In sample B no Cd is found in the bottom layer, indicating that the formation of a CdS shell around the grains could be prevented.

To verify if the formation of the CdS layers can occur without a chalcogen source, a so-called Cd-PE treatment was performed (sample C). EDX analysis revealed only a small amount of Cd within the porous bottom structure (Figure S1), but no CdS was detected. We conclude that additional sulfur is needed to form CdS. This confirms that the formation of CdS in the porous structure is possible due to the penetration of the solution containing Cd^{2+} and thiourea rather than by an ion exchange from the bulk.

For analysis of the influence of the present CdS in the porous absorber part on the electronic properties of the solar cell, EBIC measurements were performed. It visualizes the depth (*z*-direction) dependent collection of photogenerated carriers in a solar cell device (Figure 4a,b). The SEM pictures are overlaid with the EBIC signal (red). The green plot presents the integrated EBIC signal in *x*-direction at the dashed white line. The EBIC signal of sample A expands from the CZTSSe (top) to the small grains (bottom) of the CZTSSe absorber (Figure 4a). In comparison, for sample B, which has CdS deposited by PVD, the carrier collection takes place only in the top layer of the CZTSSe absorber, whereas the porous part remains passive. The EBIC signal of sample A is much broader than that for sample B. Similar behaviors of the EBIC signal were observed on different parts of the same sample (A), as well as for two other measured samples.

We suggest the following mechanism to explain the improved current generation which is schematically illustrated in Figure 4c. CdS passivates the surface of the small grains and introduces local p−n junctions within the absorber (small grains/CdS interface). The band alignment of the local p−n junction is illustrated in Figure 4d. The electron−hole pairs are effectively separated and photocurrent is generated from the porous part. Furthermore, the CdS passivation can facilitate the carrier transport within the absorber by enhancing the hole transport through the bulk of the grain toward the back contact and improves the electron transport toward the transparent conductive oxide layer via the CdS path which was formed around the grains. Finally, the CdS passivation can decrease the recombination at the small grains.

Improved charge separation and carrier transport contribute to a higher short circuit current (J_{sc}) of CdS-CBD/CZTSSe samples (Table 2). Regarding the sample where CdS was deposited by PVD, only the large grains are modified by CdS and hence carrier collection takes place only here. Visoly-Fischer et al. indicated that grain boundaries can participate in the photovoltaic processes and improve the cell performance of the CdTe cell.[13] The grain boundaries can assist in the

Table 2. Device Characteristics of CZTSSe and CIS Solar Cells[a]

sample	V_{oc} (mV)	J_{sc} (mA/cm^2)	FF (%)	Eff (%)	
CZTSSe/CBD[5]	450	30.8	59	8.3	A
CZTSSe/PVD[b]	321	24.7	50	4	B
CZTSSe/PE[b]	257	27.8	40	2.9	C
CIS/CBD	432	29.5	66	8.4	D
CZTSSe/CBD best	480	35.7	61.5	10.5	

[a]CdS was deposited by CBD or PVD. [b]Reference CBD-CdS/CZTSSe cell for the identical CZTSSe absorber has the following parameters: V_{oc} = 454 mV, J_{sc} = 26.1 mA/cm^2, FF = 43%, η = 5.1%.

DOI: 10.1021/acsami.5b02435
ACS Appl. Mater. Interfaces 2015, 7, 12141−12146

photogenerated charge separation and in the transport along the grain boundary cores.[13] Moreover, CBD-CdS gives much better surface coverage, reducing surface recombination and hence results in a higher open-circuit voltage (V_{oc}) of 454 mV in comparison to sample B with a V_{oc} = 321 mV. From Cu(In,Ga)Se_2 (CIGS) it is well-known that CBD-CdS deposition yields better device performance than PVD-CdS.[14,15] The difference in the electrical properties, in particular, the deficit in V_{oc} of the PVD-CdS CIGS, was attributed to a large lattice mismatch.[14] The CBS-CdS/CIGS interface was found not to be abrupt. It is assumed that Cu from the CIGS/CIS diffuses into the CdS layer, while Cd is incorporated into the absorber layer,[16,17] causing an inversion of the CIGS surface[18] and thus reducing recombination. Similar observations were made for the CBD-CdS/CZTS interface and a correlation of Cd and Zn diffusion and photovoltaic efficiency was reported.[19,20] Therefore, one could argue that the higher V_{oc} is due to a better junction formation at the CBD-CdS/CZTSSe interface. Table 2 summarizes the J−V device characteristics of the different samples. The solar cell performance of PE-Cd-treated CZTSSe absorber is much lower compared to that of the other CZTSSe cells. The improved J_{sc} of PE-Cd/CZTSSe interface is due to an improved collection in the shorter wavelength range, which is attributed to the reduced absorption and collection losses.

To find out if the observed formation of CdS overlayers around the small grains is common for other chalcogenide absorbers with a porous morphology, we investigated a non-vacuum-processed $CuInSe_2$ (CIS) solar cell which exhibits similar layer morphology, with large grain at the top and smaller grains and porous structure at the bottom.[11] A small amount of CdS was again found in the porous structure if CdS was deposited by CBD (Figure S2). The top layer (large grains) of the CIS layer is not sufficiently dense to prevent the penetration of the CBD solution. This observation combined with the fact that the CIS cell showed an efficiency of over 8% suggests that this phenomenon is quite universal[21] and could be expected for other non-vacuum-processed chalcogenide solar absorbers with porous bilayer morphology.

CONCLUSION

In summary, a CdS passivation layer was found around the small grains in the porous part of the DMSO solution-processed CZTSSe absorbers, which can yield up >10% efficient solar cells. The CdS layer enables the photocurrent generation even in the porous part by separation of photogenerated carriers and charge transport. The same phenomenon was observed for nanoparticle processed CIS, and could be expected for other nonvacuum chalcogenide solar cells that exhibit excessive porosity in the absorber layer.

ASSOCIATED CONTENT

Supporting Information

SEM images of TEM lamella and EDX mapping of CZTSSe solar cell device treated by Cd-PE and CIS sample. The Supporting Information is available free of charge on the ACS Publications website at DOI: 10.1021/acsami.5b02435.

AUTHOR INFORMATION

Corresponding Author

*E-mail: melanie.werner@empa.ch.

Author Contributions

#These authors contributed equally. The manuscript was written through contributions of all authors. All authors have given approval to the final version of the manuscript.

Funding

Financial support from the European Community Seventh Framework program (FP7/2007-2013) under grant agreement no. 284486 "Scalenano" is gratefully acknowledged.

Notes

The authors declare no competing financial interest.

ACKNOWLEDGMENTS

The authors would also like to thank the whole team of the Laboratory for Thin Films and Photovoltaics. Special gratitude goes to C. Gretener for the illustration. Furthermore, the authors acknowledge support of the Scientific Center for Optical and Electron Microscopy Scope M of the Swiss Federal Institute of Technology ETHZ.

REFERENCES

(1) Kim, J.; Hiroi, H.; Todorov, T. K.; Gunawan, O.; Kuwahara, M.; Gokmen, T.; Nair, D.; Hopstaken, M.; Shin, B.; Lee, Y. S.; Wang, W.; Sugimoto, H.; Mitzi, D. B. High Efficiency $Cu_2ZnSn(S,Se)_4$ Solar Cells by Applying a Double In_2S3/CdS emitter. *Adv. Mater.* **2014**, *26*, 7427−7431.

(2) Ki, W.; Hillhouse, H. W. Earth-Abundant Element Photovoltaics Directly from Soluble Precursors with High Yield Using a Non-Toxic Solvent. *Adv. Energy Mater.* **2011**, *1*, 732−735.

(3) Xin, H.; Katahara, J. K.; Braly, I. L.; Hillhouse, H. W. 8% Efficient $Cu_2ZnSn(S,Se)_4$ Solar Cells from Redox Equilibrated Simple Precursors in DMSO. *Adv. Energy Mater.* **2014**, *4*, 1301823.

(4) Schnabel, T.; Low, M.; Ahlswede, E. Solution-Processed $Cu_2ZnSn(S, Se)_4$ Solar Cells—Various Impacts on Morphology and Performance. Presented at 39th IEEE Photovoltaics Specialists Conference (PVSC 39), Tampa, Floria, June 2013; pp 0038−0042.

(5) Werner, M.; Sutter-Fella, C. M.; Romanyuk, Y. E.; Tiwari, A. N. 8.3% Efficient $Cu_2ZnSn(S,Se)_4$ Solar Cells Processed from Sodium-Containing Solution Precursors in a Closed Reactor. *Thin Solid Films* **2015**, *582*, 308−312.

(6) Chernomordik, B. D.; Béland, A. E.; Deng, D. D.; Francis, L. F.; Aydil, E. S. Microstructure Evolution and Crystal Growth in Cu_2ZnSnS_4 Thin Films Formed by Annealing Colloidal Nanocrystal Coatings. *Chem. Mater.* **2014**, *26*, 3191−3201.

(7) Collord, A. D.; Xin, H.; Hillhouse, H. W. Combinatorial Exploration of the Effects of Intrinsic and Extrinsic Defects in $Cu_2ZnSn(S,Se)_4$. Presented at 40th IEEE Photovoltaics Specialists Conference (PVSEC), Denver, Colorado, June 2014; pp 288−298.

(8) Schnabel, T.; Abzieher, T.; Friedlmeier, T. M.; Ahlswede, E. Solution-Based Preparation of $Cu_2ZnSn(S,Se)_4$ for Solar Cells, Comparison of $SnSe_2$ and Elemental Se as Chalcogen Source. *IEEE J. Photovoltaics* **2015**, *5*, 670 DOI: 10.1109/JPHOTOV.2015.2392935.

(9) Zhou, H.; Hsu, W.-C.; Duan, H.-S.; Bob, B.; Yang, W.; Song, T.-B.; Hsu, C.-J.; Yang, Y. CZTS Nanocrystals: a Promising Approach for Next Generation Thin Film Photovoltaics. *Energy Environ. Sci.* **2013**, *6*, 2822−2838.

(10) Wu, W.; Cao, Y.; Caspar, J. V.; Guo, Q.; Johnson, L. K.; Malajovich, I.; Rosenfeld, H. D.; Choudhury, K. R. Studies of the Fine-Grain Sub-Layer in the Printed CZTSSe Photovoltaic Devices. *J. Mater. Chem. C* **2014**, *2*, 3777−3781.

(11) Uhl, A. R.; Fuchs, P.; Rieger, A.; Pianezzi, F.; Sutter-Fella, C. M.; Kranz, L.; Keller, D.; Hagendorfer, H.; Romanyuk, Y. E.; LaMattina, F.; Yoon, S.; Karvonen, L.; Magorian-Friedlmeier, T.; Ahlswede, E.; VanGenechten, D.; Stassin, F.; Tiwari, A. N. Liquid-Selenium-Enhanced Grain Growth of Nanoparticle Precursor Layers for $CuInSe_2$ Solar Cell Absorbers. *Prog. Photovolt: Res. Appl.*, in press, DOI 10.1002/pip.2529.

DOI: 10.1021/acsami.5b02435
ACS Appl. Mater. Interfaces 2015, 7, 12141−12146

(12) Nichterwitz, M.; Unold, T. Numerical Simulation of Cross Section Electron-Beam Induced Current in Thin-Film Solar-Cells for Low and High Injection Conditions. *J. Appl. Phys.* **2013**, *114*, 134504.
(13) Visoly-Fisher, I.; Cohen, S. R.; Gartsman, K.; Ruzin, A.; Cahen, D. Understanding the Beneficial Role of Grain Boundaries in Polycrystalline Solar Cells from Single-Grain-Boundary Scanning Probe Microscopy. *Adv. Funct. Mater.* **2006**, *16*, 649−660.
(14) Rusu, M.; Glatzel, T.; Kaufmann, C. A.; Neisser, A.; Siebentritt, S.; Sadewasser, S.; Schedel-Niedrig, T.; Lux-Steiner, M. C. High-Efficient ZnO/PVD-CdS/Cu(In,Ga)Se_2 Thin Film Solar Cells: Formation of the Buffer-Absorber Interface and Transport Properties. Presented at 2005 MRS Spring Meeting, San Francisco, California, March−April 2005.
(15) Abou-Ras, D.; Kostorz, G.; Romeo, A.; Rudmann, D.; Tiwari, A. N. Structural and Chemical Investigations of CBD- and PVD-CdS Buffer Layers and Interfaces in Cu(In,Ga)Se_2-Based Thin Film Solar Cells. *Thin Solid Films* **2005**, *480*, 118−123.
(16) Nakada, T.; Kunioka, A. Direct Evidence of Cd Diffusion Into Cu(In, Ga)Se_2 Thin Films During Chemical-Bath Deposition Process of CdS Films. *Appl. Phys. Lett.* **1999**, *74*, 2444−2446.
(17) Ramanathan, K.; Bhattacharya, R. N.; Granata, J.; Webb, J.; Nieles, D.; Contreras, M. A.; Wiesner, H.; Hasoon, F. S.; Noufi, R. High-Efficiency Cu(In,Ga)Se_2 Thin Film Solar Cells Without Intermediate Buffer Layers. Presented at 26th IEEE Photovoltaic Specialists Conference, Anaheim, California, 1997; p 319.
(18) Chirilă, A.; Reinhard, P.; Pianezzi, F.; Bloesch, P.; Uhl, A. R.; Fella, C.; Kranz, L.; Keller, D.; Gretener, C.; Hagendorfer, H.; Jaeger, D.; Erni, R.; Nishiwaki, S.; Buecheler, S.; Tiwari, A. N. Potassium-Induced Surface Modification of Cu(In,Ga)Se_2 Thin Films for High-Efficiency Solar Cells. *Nat. Mater.* **2013**, *12*, 1107−1111.
(19) Tajima, S.; Asahi, R.; Isheim, D.; Seidman, D. N.; Itoh, T.; Hasegawa, M.; Ohishi, K. Atom-Probe Tomographic Study of Interfaces of Cu_2ZnSnS_4 Photovoltaic Cells. *Appl. Phys. Lett.* **2014**, *105*, 093901.
(20) Varley, J. B.; Lordi, V. Intermixing at the Absorber-Buffer Layer Interface in Thin-Film Solar Cells: The Electronic Effects of Point Defects in Cu(In,Ga)$(Se,S)_2$ and $Cu_2ZnSn(Se,S)_4$ Devices. *J. Appl. Phys.* **2014**, *116*, 063505.
(21) Scragg, J. J.; Berg, D. M.; Dale, P. J. A 3.2% Efficient Kesterite Device from Electrodeposited Stacked Elemental Layers. *J. Electroanal. Chem.* **2010**, *646*, 52−59.

DOI: 10.1021/acsami.5b02435
ACS Appl. Mater. Interfaces 2015, 7, 12141−12146